

Reactive oxygen species regulate F-actin dynamics in neuronal growth cones and neurite outgrowth

Vidhya Munnamalai* and Daniel M. Suter*†

*Department of Biological Sciences, Purdue University, West Lafayette, Indiana, USA

†Bindley Bioscience Center, Purdue University, West Lafayette, Indiana, USA

Abstract

Reactive oxygen species are well known for their damaging effects due to oxidation of lipids, proteins and DNA that ultimately result in cell death. Accumulating evidence indicates that reactive oxygen species also have important signaling functions in cell proliferation, differentiation, cell motility and apoptosis. Here, we tested the hypothesis whether reactive oxygen species play a physiological role in regulating F-actin structure and dynamics in neuronal growth cones. Lowering cytoplasmic levels of reactive oxygen species with a free radical scavenger, *N*-tert-butyl- α -phenylnitrone, or by inhibiting specific sources of reactive oxygen species, such as NADPH oxidases or lipoxygenases, reduced the F-actin content in the peripheral domain of growth cones. Fluorescent

speckle microscopy revealed that these treatments caused actin assembly inhibition, reduced retrograde actin flow and increased contractility of actin structures in the transition zone referred to as arcs, possibly by activating the Rho pathway. Reduced levels of reactive oxygen species ultimately resulted in disassembly of the actin cytoskeleton. When neurons were cultured overnight in conditions of reduced free radicals, growth cone formation and neurite outgrowth were severely impaired. Therefore, we conclude that physiological levels of reactive oxygen species are critical for maintaining a dynamic F-actin cytoskeleton and controlling neurite outgrowth.

Keywords: actin dynamics, growth cone, neurite outgrowth, reactive oxygen species, Rho, signaling.

J. Neurochem. (2009) **108**, 644–661.

Reactive oxygen species (ROS), such as superoxide $O_2^{\bullet-}$, hydrogen peroxide H_2O_2 and the hydroxyl radical OH^{\bullet} , are by-products of the electron transport chain in mitochondria but are also specifically produced by a number of membrane-bound and cytosolic oxidases, including NADPH oxidase, lipoxygenase and xanthine oxidase (Thannickal and Fanburg 2000; Bedard and Krause 2007). At very high concentrations ROS can negatively impact cell structure and function by oxidation of lipids, proteins and DNA, which occurs in cancer, atherosclerosis, diabetes and neurodegenerative disorders. In the nervous system, toxic effects of ROS have been reported for spinal cord injury (Luo *et al.* 2002; Xu *et al.* 2005), glutamate excitotoxicity (Reynolds and Hastings 1995; Duan *et al.* 2007), and Alzheimer's and Parkinson's disease (Tabner *et al.* 2001). Since neurons have a very high rate of oxygen consumption and oxidative phosphorylation, they are particularly susceptible to ROS-induced damage. However, the high oxygen consumption could also indicate that neurons use ROS in intracellular signaling during apoptosis, differentiation and cell migration (Maher and Schubert 2000; Thannickal and Fanburg 2000).

Recent studies have shed light on a physiological role of ROS in regulating cell motility and adhesion, particularly of vascular endothelial cells and fibroblasts (Moldovan *et al.* 2006; Chiarugi and Fiaschi 2007). For example, wound healing assays have shown that motile endothelial cells exhibit higher ROS levels than stationary cells and that actin polymerization and cell migration correlate with ROS production (Moldovan *et al.* 2000). Furthermore, ROS mediate integrin-dependent cell adhesion, spreading and

Received July 31, 2008; revised manuscript received October 12, 2008; accepted November 10, 2008.

Address correspondence and reprint requests to Daniel Suter, Department of Biological Sciences, Purdue University, 915 West State Street, West Lafayette, IN 47907-2054, USA.

E-mail: dsuter@purdue.edu

Abbreviations used: ASW, artificial seawater; C, central; DCFH-DA, 2',7'-dichlorofluorescein diacetate; DIC, differential interference contrast; DMSO, dimethylsulfoxide; FSM, fluorescent speckle microscopy; LPA, oleoyl-L- α -lysophosphatidic acid sodium salt; MnTBAP, Mn(III) tetrakis(4-benzoic acid) porphyrin chloride; NA, numerical aperture; NDGA, nordihydroguaiaretic acid; P, peripheral; PAO, phenyl arsine oxide; PBN, *N*-tert-butyl- α -phenylnitrone; PY, phosphotyrosine; ROS, reactive oxygen species; T, transition; tBHP, tert-butyl hydroperoxide.

related actin reorganization in NIH-3T3 fibroblasts (Chiarugi *et al.* 2003; Fiaschi *et al.* 2006). However, the detailed mechanisms of how ROS affect structure and dynamics of the actin cytoskeleton in these non-neuronal cells are unknown. The small GTPases of the Rho family (Etienne-Manneville and Hall 2002) are key suspects in mediating ROS-dependent actin reorganization. Rac1 not only regulates actin assembly but also increases intracellular ROS levels by activating either certain NADPH oxidase complexes (Abo *et al.* 1991) or the cytosolic phospholipase A₂/arachidonic acid/lipoxygenase-cascade (Woo *et al.* 2000). A pathway involving redox-dependent down-regulation of Rho activity by Rac involving low-molecular-weight protein tyrosine phosphatases and p190 Rho GTPase activating protein has been established for integrin-mediated cell spreading of HeLa cells (Nimnual *et al.* 2003). Additional studies in endothelial cells and fibroblasts implicated Rac1 and RhoA in ROS-mediated actin reorganization (Wojciak-Stothard *et al.* 2005; Alexandrova *et al.* 2006).

Rho GTPases also regulate actin structure and dynamics in growth cone motility and guidance (Giniger 2002; Gallo and Letourneau 2004). While Cdc42 and Rac1 mediate filopodial growth and lamellipodial protrusion, respectively, RhoA induces growth cone collapse and axon retraction, for example by regulating actomyosin-contractility of actin arcs in the transition (T) zone (Zhang *et al.* 2003; Gallo and Letourneau 2004; Gallo 2006). Actin arcs are oriented perpendicular to the filopodial actin bundles and emerge in the T zone from the retrogradely-moving lamellipodial actin networks (Schaefer *et al.* 2002; Zhang *et al.* 2003). The possibility that physiological ROS levels are vital for regulating F-actin structure and dynamics in growth cones, potentially via Rho GTPases, and thereby control growth cone motility and neurite outgrowth is a provocative and novel idea. Here, we tested this hypothesis by reducing growth cone ROS levels in two major ways: (i) by generally decreasing free radicals with the scavenger *N*-tert-butyl- α -phenylnitron (PBN), and (ii) by inhibiting specific cellular sources of free radicals: NADPH oxidases using phenyl arsine oxide (PAO) and apocynin, lipoxygenases by nordihydroguaiaretic acid (NDGA) treatment, and complex I of the mitochondrial electron transport chain by rotenone. Both general and NADPH oxidase- and lipoxygenase-specific ROS depletions resulted in significantly reduced F-actin content in *Aplysia* growth cones. Using fluorescent speckle microscopy (FSM) of F-actin dynamics, we observed reduced actin assembly and retrograde flow as well as increased arc contractility and disassembly of the F-actin cytoskeleton in the peripheral (P) domain. ROS depletion resulted in Rho activation, reduced growth cone formation and neurite outgrowth. Therefore, ROS may have a two-faced role in the nervous system: while at high concentrations ROS are harmful to neurons, at physiological levels they are critical for normal F-actin dynamics and neurite outgrowth.

Materials and methods

ROS reagents

Apocynin (4'-hydroxy-3'-methoxyacetophenone), 2',7'-dichlorofluorescein diacetate (DCFH-DA), oleoyl-L- α -lysophosphatidic acid (LPA) sodium salt, NDGA, *N*-tert-butyl hydroxylamine acetate, PAO, PBN, tert-butyl hydrogen peroxide (tBHP) and rotenone were purchased from Sigma-Aldrich (St. Louis, MO, USA). Mn (III) tetrakis (4-benzoic acid) porphyrin chloride (MnTBAP) was from Alexis Biochemicals (San Diego, CA, USA). DCFH-DA was prepared as 15.5 mM stock in dimethylsulfoxide (DMSO). PAO (20 mM), apocynin (2 M), and NDGA (0.5 M) were prepared as stocks in DMSO, and appropriate controls were included in all experiments (e.g., 0.005% DMSO for 1 μ M PAO). PBN and tBHP solutions were prepared in artificial seawater (ASW: 400 mM NaCl, 10 mM KCl, 10 mM CaCl₂, and 55 mM MgCl₂, 15 mM HEPES at pH 7.8) or L15-ASW, while LPA (20 mM) and MnTBAP (0.1 M) were dissolved as stocks in H₂O. Rotenone was prepared as 8 M stock in EtOH. For live-cell imaging, ROS reagents were applied in ASW, unless otherwise noted.

Aplysia bag cell neuronal culture

Aplysia bag cell neurons were plated on coverslips coated with 20 μ g/mL poly-L-lysine (70–150 kDa) as previously described (Suter *et al.* 1998; Lee *et al.* 2008). Cells were kept in L15 medium (Invitrogen, Carlsbad, CA, USA) supplemented with ASW (L15-ASW: L15 plus 400 mM NaCl, 10 mM CaCl₂, 27 mM MgSO₄, 28 mM MgCl₂, 4 mM L-glutamine, 50 μ g/mL gentamicin, 5 mM HEPES, pH 7.9) overnight in a 14°C incubator. All procedures were performed in accordance with institutional guidelines. Neurons were typically used for experiments 24 h after plating.

Differential interference contrast and immunofluorescence microscopy

Differential interference contrast (DIC) imaging was performed with a 60 \times 1.4 numerical aperture (NA) oil objective (plus 1.5 \times magnification) on an Eclipse TE2000 microscope (Nikon, Melville, NY, USA), using either a Cascade II or a CoolSNAP HQ CCD camera (Photometrics, Tucson, AZ, USA) controlled by MetaMorph 7 software (Molecular Devices, Downingtown, PA, USA). DIC images were acquired with 25–100 ms exposure times at 10 s intervals through an OG 590 long-pass red filter (Chroma, Rockingham, VT, USA). Growth cones were imaged under control condition in ASW for 10 min, then in the presence of ROS reagents for 10–20 min. F-actin and microtubule labeling was carried out as described (Suter *et al.* 2004). Alexa 488-phalloidin (Invitrogen) was used at 1 : 100 for F-actin. Mouse anti- α -tubulin (Sigma) was incubated at 0.7 μ g/mL in 5% bovine serum albumin/phosphate-buffered saline/0.1% Triton X-100 for 1 h at RT, followed by 4 μ g/mL Alexa 568-goat-anti-mouse secondary antibody (Invitrogen) in the same blocking solution for 30 min at RT. Phosphotyrosine (PY) staining was performed with the monoclonal antibody 4G10 (Millipore, Billerica, MA, USA) at 2 μ g/mL in the blocking solution above for 1 h at RT, followed by the same secondary antibody as for the tubulin staining. Images were acquired in 20 mM *n*-propyl-gallate in phosphate-buffered saline/80% glycerol pH 8.5 on a Nikon TE2000 Eclipse microscope equipped with a 60 \times 1.4 NA oil and 100 \times 1.49 NA oil objectives,

an X-cite 120 metal halide lamp (EXFO, Mississauga, Ontario, Canada), appropriate fluorescence filter sets (Chroma), Cascade II cooled CCD camera (200–500 ms exposure times) and MetaMorph 7 software.

ROS imaging

Neurons were incubated with 5 μ M DCFH-DA in ASW with or without drug for 15 min at RT and then washed with ASW. Dichlorofluorescein (DCF)-images were acquired through a FITC filter set using the Cascade II camera (500 ms exposure time). For ratiometric ROS imaging, the volume indicator Texas Red-dextran (3 kDa, Invitrogen) was microinjected into cell bodies at a concentration of 2 mg/mL in RNase-free water. Dextran images were taken with a TexasRed filter set. DCF intensity values in the P domains of the growth cones were background subtracted and normalized against dextran signals. Data were collected from 11 to 40 growth cones.

Quantitative actin fluorescent speckle microscopy

For quantitative FSM of actin dynamics, neuronal cell bodies were microinjected with 20 μ M Alexa 568 phalloidin (Invitrogen), in injection buffer (100 mM PIPES pH 7.0, 1 mM MgCl₂, 1 mM EGTA) as recently described (Schaefer *et al.* 2002). In some experiments, we used Alexa 568-labeled G-actin (Invitrogen) to monitor actin dynamics. While actin arcs and bundles are more easily discerned with phalloidin, we did not measure any differences in the dynamic properties of the actin cytoskeleton between the two probes. Reagents were injected, using an NP-2 micromanipulator and Femtojet microinjection system (Eppendorf, New York, NY, USA). After injection, cells were allowed to recover for 1 h before time-lapse imaging in ASW (500 ms exposure times at 10 s intervals using the Cascade II). For LPA treatment, 20 μ M LPA was dissolved in a low-ionic strength ASW solution (LIS-ASW; 15 mM HEPES, pH 7.9, 60 g/L glycine, 100 mM NaCl, 10 mM KCl, 5 mM MgCl₂, 5 mM EGTA).

Image processing and analysis

MetaMorph 7.0 was used for image processing, quantitative analysis of actin dynamics and making of movies and montages. To enhance actin speckles, images were processed with an unsharp mask, then with a low-pass filter. The MetaMorph kymograph function was used to measure retrograde actin flow rates along 5–10 F-actin bundles to determine the average flow rate per growth cone. To measure actin arc movements in the T zone, 4–7 actin speckles per growth cone were tracked at 10 s intervals. The average angle between the direction of arc movements and the axis of growth was determined for each growth cone and treatment. In order to measure arc density in the T zone, lines scans were drawn across arcs on the sides of the growth cone, and profiles were compared between control and PBN conditions. For statistical analysis of arc density, 2–3 line scan measurements were made per growth cone, and integrated fluorescence intensity values per μ m in drug condition were normalized against integrated values in control condition and averaged. One-tailed paired *t*-tests were performed to identify significant differences. Photoshop CS3 extended (Adobe, San Jose, CA, USA) was used for additional image processing and making of supplemental videos, and Canvas 8 (ACD Systems of America Inc., Miami, FL, USA) for final figure assembly.

Quantification of growth cone formation and neurite outgrowth

Aplysia bag cell neurons were plated in L15-ASW medium on day 0. After 2–3 h of incubation at RT, the medium was replaced with L15-ASW with or without ROS reagents. On day 1, 10 \times phase images were taken of each cell, followed by a thorough washout with L15-ASW. On day 2, 10 \times phase images were taken of each cell again after drug was washed out 1 day before. To assess growth cone formation, the percentage of cells containing growth cones was determined for each condition on day 1 and day 2 in two independent experiments (70–255 cells per condition). In the neurite outgrowth assay, total neurite length was determined on day 1 and day 2. A population distribution of the percentage of neurons with a total neurite length greater than a specific length was plotted against total neurite length (Chang *et al.* 1987).

Rho activity assay

To assess Rho activity in *Aplysia* CNS tissue, we adapted a previously described protocol (Zhang *et al.* 2003). Rho activity assay kit was purchased from Cytoskeleton Inc. (Denver, CO, USA). In brief, *Aplysia* CNS tissue was incubated for 6 h with 6 mg/mL dispase II (Roche, Indianapolis, IN, USA) in L15-ASW to assist penetration of drug. CNS tissue was washed three times with ice-cold ASW and then incubated with LIS-ASW with 20 μ M LPA, 75 mM PBN or without drug for 1 h at RT. Each tissue sample was lysed for 10 min on ice, using the lysis buffer supplied by the kit. After homogenization with a handheld homogenizer (Omni International, Marietta, GA, USA), lysates were cleared by centrifugation at 12 000 *g* for 5 min at 4°C. Extracts were incubated with agarose beads coupled with glutathione S-transferase-tagged Rho binding domain of rhotekin for 1 h at 4°C. Beads were washed with the provided wash buffer, boiled in sample buffer for 5 min at 95°C and analyzed by 15% sodium dodecyl sulfate-polyacrylamide gel electrophoresis. The amounts of total Rho and active Rho were quantified by western blotting with the mouse monoclonal antibody p1D9 (1 : 10 dilution of supernatant; Developmental Studies Hybridoma Bank, University of Iowa, Iowa City, IA, USA). We used the secondary antibody Alexa 680-goat-anti-mouse (Invitrogen) at 0.4 μ g/mL, followed by detection with the Odyssey system (LI-COR Biosciences, Lincoln, NE, USA). Band intensities were quantified with the Odyssey software.

Results

ROS levels in neuronal growth cones

To investigate whether physiological ROS levels regulate F-actin structure and dynamics in neuronal growth cones, we selected two different approaches to decrease intracellular ROS. (i) We treated cultured *Aplysia* bag cell neurons with the spin-trapping reagent PBN, a general free radical scavenger that has been used to detect ROS in the brain as well as to reduce radical-mediated neuronal damage (Zini *et al.* 1992; Thomas *et al.* 1997). (ii) We also inhibited specific intracellular ROS sources, such as NADPH oxidases with PAO (Le Cabec and Maridonneau-Parini 1995) and apocynin (Stolk *et al.* 1994), lipoxygenases with NDGA (Salari *et al.* 1984), and the mitochondrial electron transport

chain complex I by rotenone (Barrientos and Moraes 1999). In order to verify that our experimental treatments indeed decreased ROS, we measured the relative cytoplasmic ROS levels in growth cones with DCFH-DA (Fig. 1).

Figure 1(a) shows a DIC image of a control growth cone, revealing the three major growth cone regions: central (C) domain, T zone and P domain. DCF imaging showed that ROS are present in all three domains in a volume-dependent manner when comparing the DCF signal to the distribution of Texas Red dextran serving as a volume control (Fig. 1b and c). ROS levels are the highest in the C domain, particularly in punctate and elongated structures likely to be mitochondria (arrows in Fig. 1b and d). Weaker signals were observed in network-like structures in the C domain and T zone, which are most likely endoplasmic reticulum (Fig. 1b). The lowest ROS levels were detected in the P domain (Fig. 1b). Incubation of *Aplysia* bag cell neurons with 500 nM DCFH-DA for as short as 5 min resulted in measurable signals, suggesting that they are highly oxidative cells. Treatment of growth cones with 50 mM PBN, 1 μ M PAO, 4 mM apocynin or 50 μ M NDGA for 15 min significantly reduced cytoplasmic ROS levels in the P domain (Fig. 1d–g), while 20 μ M rotenone had no effects on cytoplasmic DCF signals (Fig. 1h).

We quantified ROS levels in the relatively thin P domain (Grzywa *et al.* 2006) by normalizing DCF intensity values to Texas Red dextran signals to correct for potential volume changes induced by the drugs (Fig. 1j). PBN, PAO, apocynin, and NDGA treatment significantly reduced cytoplasmic ROS levels in the P domain when compared to control treatments: 67% by 50 mM PBN, 74% by 1 μ M PAO, 54% by 4 mM apocynin, and 50% by 50 μ M NDGA. Growth cones treated with 20 μ M rotenone had a small and insignificant increase of cytoplasmic DCF signals of 13%, while mitochondrial DCF levels in the P domain were clearly reduced by 63% when compared to controls (data not shown). In addition, we observed a dose-dependent reduction of cytoplasmic ROS levels when treating the cells with 25, 50 and 75 mM PBN. Previous studies reported non-toxic, radical-scavenging effects of 10 mM PBN in cultured macrophages, lymphoma cells and neurons, respectively (Kotake *et al.* 1998; Sturgess *et al.* 2000; Cui *et al.* 2006). The higher concentrations of PBN needed to reduce ROS levels in *Aplysia* neurons compared to vertebrate cells are consistent with our experience using other pharmacological reagents in this system. As a positive control, we treated the neurons with 5 mM tBHP, a membrane permeable H₂O₂ variant, and we found significantly increased DCF signals in all growth cone domains (Fig. 1i and j; 3.7-fold increase in the P domain when compared with control). In summary, DCF imaging revealed that both NADPH oxidases and lipoxygenases, but not mitochondria, are major sources of ROS in the P domain of the growth cone.

ROS depletion reduces F-actin content in neuronal growth cones

We next studied the effects of ROS depletion on growth cone morphology and the distribution of F-actin and microtubule cytoskeleton (Figs 2 and 3). In the P domain, F-actin is present in filopodial bundles (arrow in Fig. 2a-ii; schematic in upper left) as well as in a lamellipodial network between the filopodia (Forscher and Smith 1988; Lewis and Bridgman 1992). The T zone contains dynamic ruffling structures called ‘intrapodia’ (Rochlin *et al.* 1999) (asterisk in Fig. 2a-ii), as well as transverse actin arcs surrounding the C domain (arrow in Fig. 2b-iii) that derive from the peripheral actin network and undergo Rho-dependent actomyosin contractility (Schaefer *et al.* 2002; Zhang *et al.* 2003). The majority of the microtubules are present in the C domain, while highly dynamic microtubules explore the P domain by using actin bundles as polymerization guides (Fig. 2a-ii) (Schaefer *et al.* 2002).

When growth cones were treated with 25 mM PBN for 20 min, we observed an initial burst of filopodial growth, flattening of the P domain, loss of membrane ruffling in the T zone, and forward movement of the C domain boundary towards the leading edge (Fig. 2b-ii; Video S1). All these effects were completely reversible following PBN washout (data not shown). Phalloidin-labeling following fixation revealed that the F-actin cytoskeleton was strongly affected by PBN treatment: we observed fewer filopodial bundles and intrapodia as well as less actin meshwork when compared to control conditions (Fig. 2b-iii). Microtubules, on the other hand, extended into the P domain with reduced F-actin content, similarly to growth cones treated with the actin depolymerizing drug cytochalasin B (Forscher and Smith 1988).

There is recent evidence for ROS-mediated down-regulation of Rho activity in HeLa cells (Nimnual *et al.* 2003). If a similar signal transduction pathway would occur in growth cones, we would expect an increase in arc contractility in the T zone upon lowering ROS levels. Although arcs were clearly visible after treatment with 25 mM PBN (arrow in Fig. 2b-iii), extension of the C domain did not suggest a strong contractile effect at these ROS levels. Thus, Rho-activation might need a more significant reduction of ROS levels. When growth cones were incubated with 75 mM PBN for 5 min, we also noticed reduced T zone ruffling; however, no initial filopodial extension occurred, and the C domain boundary did not extend and sometimes retracted (Fig. 2c-ii; Video S2). Overall, growth cone and organelle dynamics was severely affected in 75 mM PBN. F-actin content was strongly reduced in the P domain, which was invaded by microtubules as observed with 25 mM PBN (Fig. 2c-iii). Similar effects on growth cone morphology and F-actin structures were observed with other ROS scavengers such as 30 mM *N*-tert butyl hydroxylamine acetate and 0.2 mM MnTBAP (data not shown), a superoxide dismutase mimetic (Patel 1998).

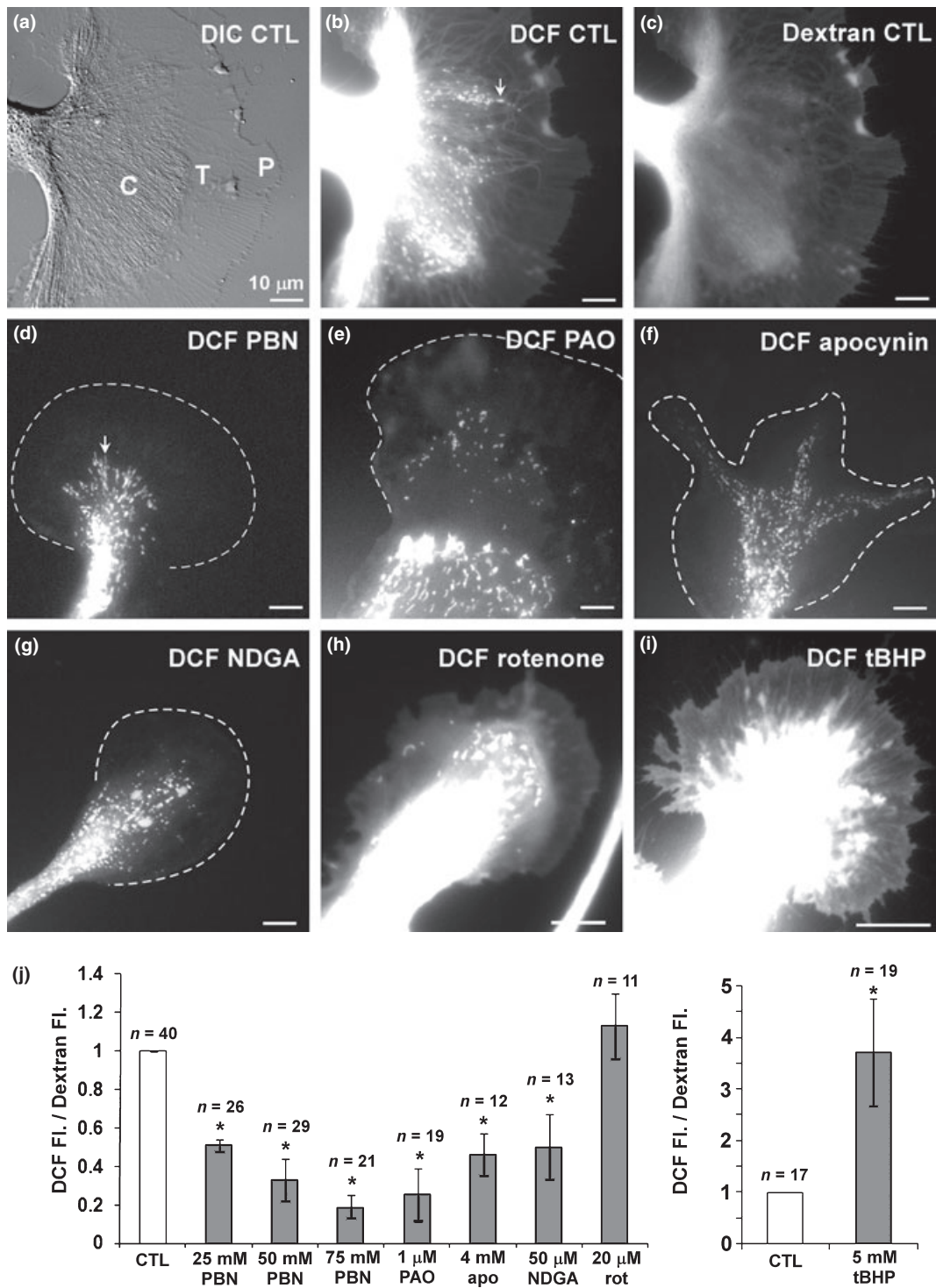


Fig. 1 ROS imaging in *Aplysia* bag cell growth cones. (a) DIC image of a control (CTL) growth cone. P and C domain plus T zone are indicated. (b) DCF image of growth cone in (a) shows ROS levels in the cytoplasm as well as intracellular compartments, such as potential mitochondria (arrow). (c) Corresponding dextran fluorescence image reveals highest volume in the C domain. (d–i) DCF fluorescence

images of growth cones treated for 15 min with 50 mM PBN (d), 1 μM PAO (e), 4 mM apocynin (apo) (f), 50 μM NDGA (g), 20 μM rotenone (rot) (h), or 5 mM tBHP (i), respectively. Leading edges of growth cones shown in (d–g) are marked with dashed line. (j) Quantification of volume-corrected ROS levels in the growth cone P domain. *T*-test: **p* < 0.05 (*n* = growth cones). Scale bars: 10 μm.

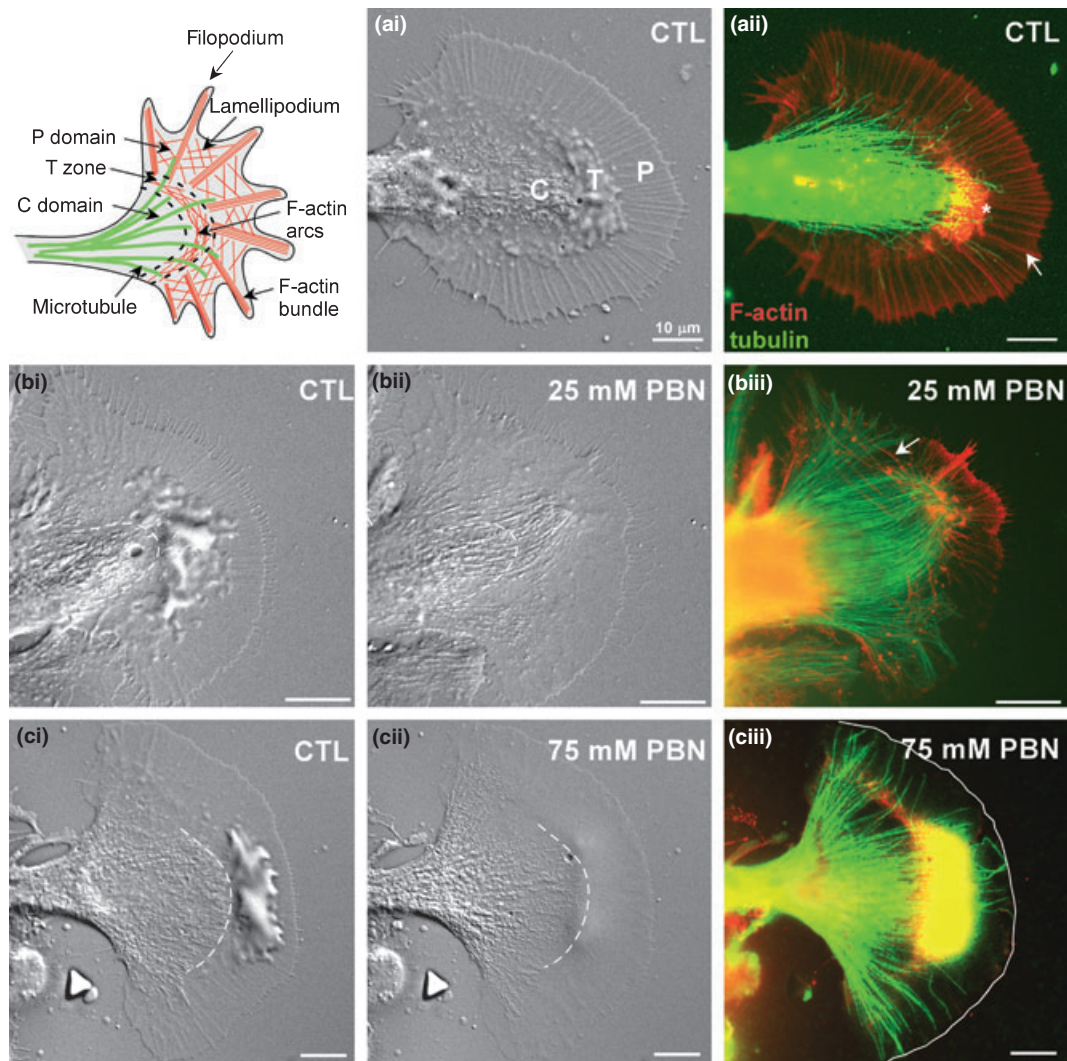


Fig. 2 ROS depletion decreases F-actin content in growth cones. Upper left inset shows schematic of cytoplasmic domains, microtubules (green) and F-actin (red) subpopulations in the growth cone. (a-i) DIC image of a live control growth cone under control condition in ASW. (a-ii) Overlay image of F-actin (red) and microtubule (green) double labeling after fixation of growth cone in (a-i) shows filopodial F-actin bundles (white arrow) and an F-actin meshwork between filopodia in the P domain. Intrapodia in the T zone is marked with an asterisk. The C domain is rich in organelles and microtubules. (b:i-iii)

25 mM PBN treatment (20 min) decreased membrane ruffling and caused initial filopodial lengthening and extension of the C domain boundary (dashed line in b-ii; Video S1). The F-actin content was strongly reduced while microtubule extended into the P domain (b-iii). Arrow points towards actin arc. (c:i-iii) 75 mM PBN treatment (5 min) also reduced ruffling (c-ii; Video S2) and strongly depleted F-actin structures (c-iii, leading edge marked with solid line). Scale bars: 10 μ m.

Since membrane-actin interactions are important for growth cone motility, we suspected that plasma membrane-bound NADPH oxidase (Bedard and Krause 2007; Lambeth 2007) could be an important ROS source for actin regulation in growth cones. Treatments with two different NADPH oxidase inhibitors, 1 μ M PAO and 4 mM apocynin, for 10 min or longer resulted in flattening of the P domain and decreased membrane ruffling (Fig. 3a-i,ii and b-i,ii; Videos S3 and S4). Treatments with 25 mM PBN, 1 μ M PAO and 4 mM apocynin had overall similar effects,

although we did not observe an initial burst of filopodial growth with PAO. Furthermore, the C domain boundary rather retracted with PAO treatment. F-actin bundles and meshwork in the P domain were significantly reduced by both PAO and apocynin, while microtubules remained intact and invaded the P domain (Fig. 3a-iii and b-iii). We also inhibited ROS production by cytosolic lipoxygenases with 50 μ M NDGA. Consistent with PBN, PAO and apocynin treatments, NDGA also caused flattening of the P domain and T zone, accompanied by a loss of F-actin

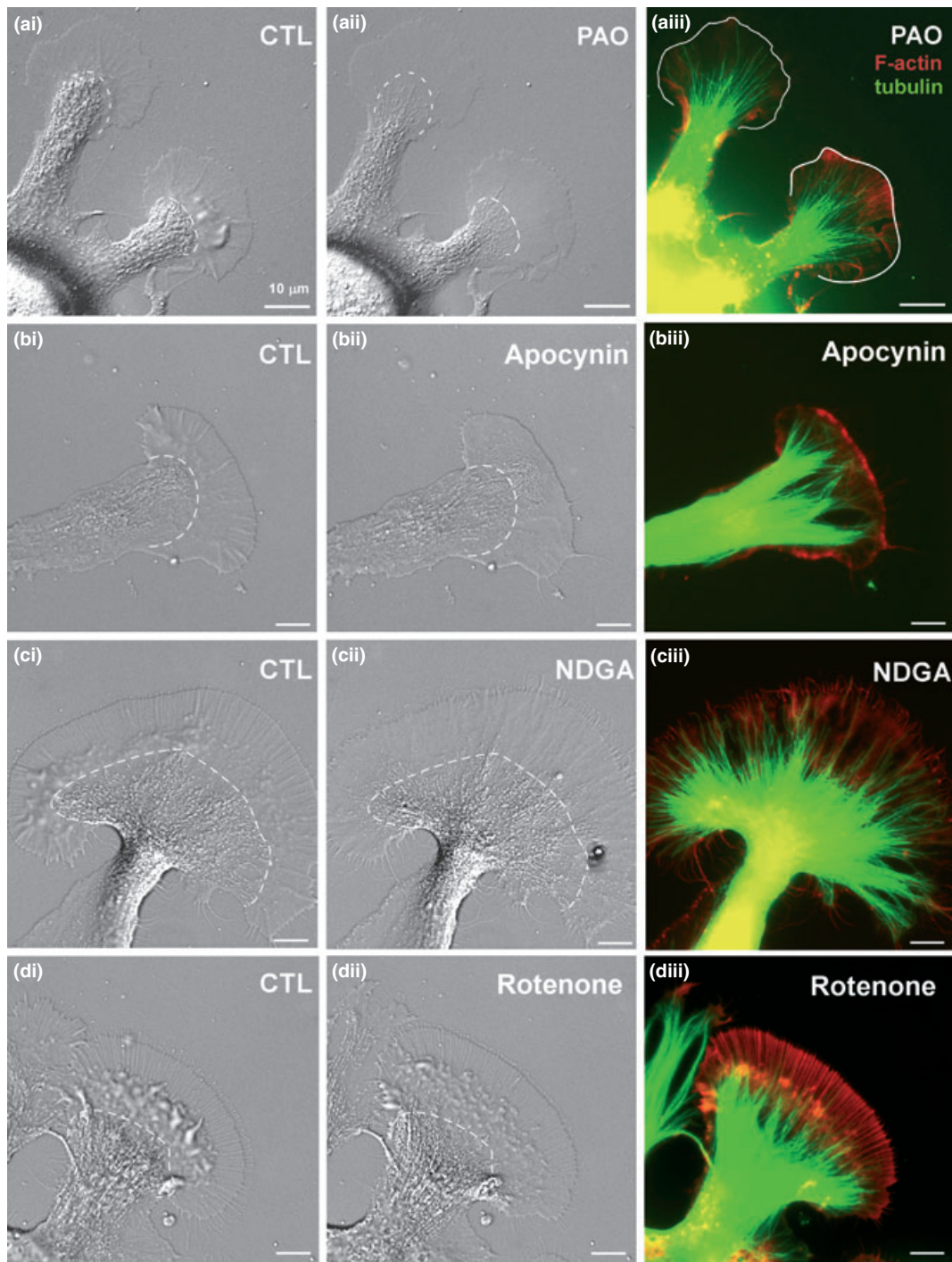


Fig. 3 Inhibition of NADPH oxidases and lipoxygenases decreases F-actin content. (a:i–iii) NADPH oxidase inhibition by 1 μM PAO (10 min) caused flattening of the P domain and T zone and a slight C domain retraction (a-ii). Growth cone dynamics including actin retrograde flow was strongly reduced (Video S3). (a-iii) F-actin bundles and meshwork in the periphery were reduced and microtubules extended more towards the leading edge (marked with solid line). (b:i–iii) 4 mM apocynin treatment (10 min) resulted in flattening of P domain and the T zone as well as extension of the C domain (b-ii; Video S4). (b-iii) The

actin bundles and meshwork in the P domain were decreased and microtubules extended into the actin-free periphery. (c:i–iii) 50 μM NDGA treatment (10 min) had similar effects on growth cones. The extension of the C domain was modest. There was significant filopodia elongation (c-ii, Video S5). (c-iii) NDGA treatment decreased F-actin content in the P domain, but elongated filopodia containing F-actin. (d:i–iii) 20 μM Rotenone treatment (10 min) did not result in significant changes in growth cone morphology, F-actin and microtubule cytoskeleton structure and content (Video S6). Scale bars: 10 μm.

bundles in the P domain (Fig. 3c; Video S5). We also noticed a significant elongation of F-actin-containing filopodia in the presence of NDGA (Fig. 3c; Video S5). In contrast, when complex I of the mitochondrial electron transport chain was inhibited with 20 μ M rotenone, the only morphological change observed was a slight splaying of the C domain (Fig. 3d-ii; Video S6), while both F-actin and microtubule cytoskeleton remained unaffected (Fig. 3d-iii). In summary, our results suggest that physiological levels of ROS that are largely derived from NADPH oxidases and lipoxygenases, are crucial for maintaining an intact F-actin cytoskeleton in the P domain of neuronal growth cones.

ROS depletion affects F-actin dynamics and contractility

In order to assess which specific aspects of F-actin dynamics are affected by ROS depletion, we used actin FSM (Figs 4 and 5; Videos S7–S12) (Waterman-Storer *et al.* 1998; Schaefer *et al.* 2002). In control conditions, filopodial actin bundles and intervening lamellipodial networks are constantly turning over by coordinated assembly at filopodia tips and the leading edge, retrograde flow at the rate of $4.6 \pm 0.4 \mu\text{m}/\text{min}$ ($n = 11$ growth cones) and recycling in the T zone (Fig. 4a; Video S7). When growth cones were treated with 25 mM PBN, we observed an initial burst of filopodial growth, a progressive disassembly of actin filaments in bundles and networks, as well as the forward movement of the actin recycling zone that resulted in a narrower P domain (arrowhead in Fig. 4b; Video S7). Kymograph analysis revealed a retraction of the leading edge and a 52% decrease in retrograde actin flow after 20 min treatment with 25 mM PBN compared to controls (Fig. 4b, c and i). These results suggest an inhibition of actin assembly at the leading edge when lowering ROS levels. Ultimately, all F-actin structures including arcs progressively disappeared in 25 mM PBN (Video S7). Thus, the C domain extension induced by 25 mM PBN could be because of fewer actin arcs in the T zone that keep the C domain boundary compact under control condition.

Upon treatment with 75 mM PBN, strong actin assembly inhibition and increased contractility were observed before significant flow reduction and network disassembly occurred (Fig. 4j; Video S11). Such treatment resulted in a fast retraction of the peripheral F-actin cytoskeleton into the C domain at a rate of $5.4 \mu\text{m}/\text{min}$, which is comparable to control actin flow rates. The clearance of P domain F-actin with 75 mM PBN is reminiscent of the effect of the actin depolymerizing drug cytochalasin B on *Aplysia* growth cones (Forscher and Smith 1988). Such strong reduction of ROS levels also resulted in pulling apart of actin networks (Video S11) and in aggregation of actin arcs, both of which are signs of increased contractility (Fig. 4j). Arc aggregation was also observed upon treatment with 0.2 mM MnTBAP (Fig. 4k).

When NADPH oxidases were inhibited with either 1 μ M PAO or 4 mM apocynin, actin dynamics was affected similarly as with 25 mM PBN. After about 15 min of treatment, PAO and apocynin decreased actin flow rates by 73% and 65%, respectively, and this was accompanied by a brief period of leading edge protrusion and lengthening of filopodial actin bundles (Fig. 4e–g and i; Videos S8 and S9). Ultimately, filopodial actin assembly was also inhibited, the actin recycling zone moved forward, and the highly structured filopodia and lamellipodia were replaced with a disorganized meshwork (Videos S8 and S9). NDGA treatment reduced actin flow rates by 33% when compared to controls (Fig. 4i); however, filopodia elongated and persisted in length in NDGA (Figs 3c-iii and 4h; Video S10). Furthermore, NDGA caused aggregation and increased contractility of actin arcs, similar to 75 mM PBN treatment (Fig. 4h and j, Videos S10 and S11). In summary, all treatments that reduced ROS levels resulted in decreased actin flow, inhibition of actin assembly along the leading edge, and progressive disassembly of the actin meshwork in the P domain. In addition, lipoxygenase-inhibition increased actomyosin-based contractility.

ROS depletion affects actin arc movement and aggregation

The increased actomyosin contractility induced by either 75 mM PBN or 50 μ M NDGA was indicated by C domain contraction, pulling apart of actin networks and increased arc density (Fig. 4h and j; Videos S10 and S11). We quantified these changes in arc dynamics and structure in more detail (Fig. 5). In control conditions, arcs moved towards the C domain retrogradely relative to the direction of growth (Fig. 5a and b; Videos S11 and S12). New arcs are constantly formed from actin networks in the P domain, as previously reported (Schaefer *et al.* 2002; Zhang *et al.* 2003). Immediately after PBN addition, arcs started to aggregate and were tugged towards the direction of growth (Fig. 5c and d; Videos S11 and S12). By tracking actin speckles on arcs, we found that in control condition arcs were always moving retrogradely at angles greater than 90° with respect to the axis of growth (average angle $140^\circ \pm 9^\circ$; $n = 6$), while after PBN treatment angles were below 90° (average angle $46^\circ \pm 8^\circ$; $n = 7$; Fig. 5e and f).

Rho activation by lysophosphatidic acid (LPA) increases arc contractility and density in *Aplysia* growth cones (Zhang *et al.* 2003). ROS depletion by PBN and NDGA resulted in arc aggregation similarly to growth cones treated with 20 μ M LPA for 15 min (Fig. 4h and j; Fig. 5a–d, g, h; Videos S10 and S11). In contrast to PBN and NDGA, LPA did not cause a retraction of the P domain F-actin structures into the C domain nor a network disruption by disorganized force application or F-actin disassembly. We quantified arc aggregation induced by PBN, LPA and NDGA treatment by intensity line-scan analysis across actin arcs on the side of growth cones (Fig. 5i and j). In all three conditions, we found

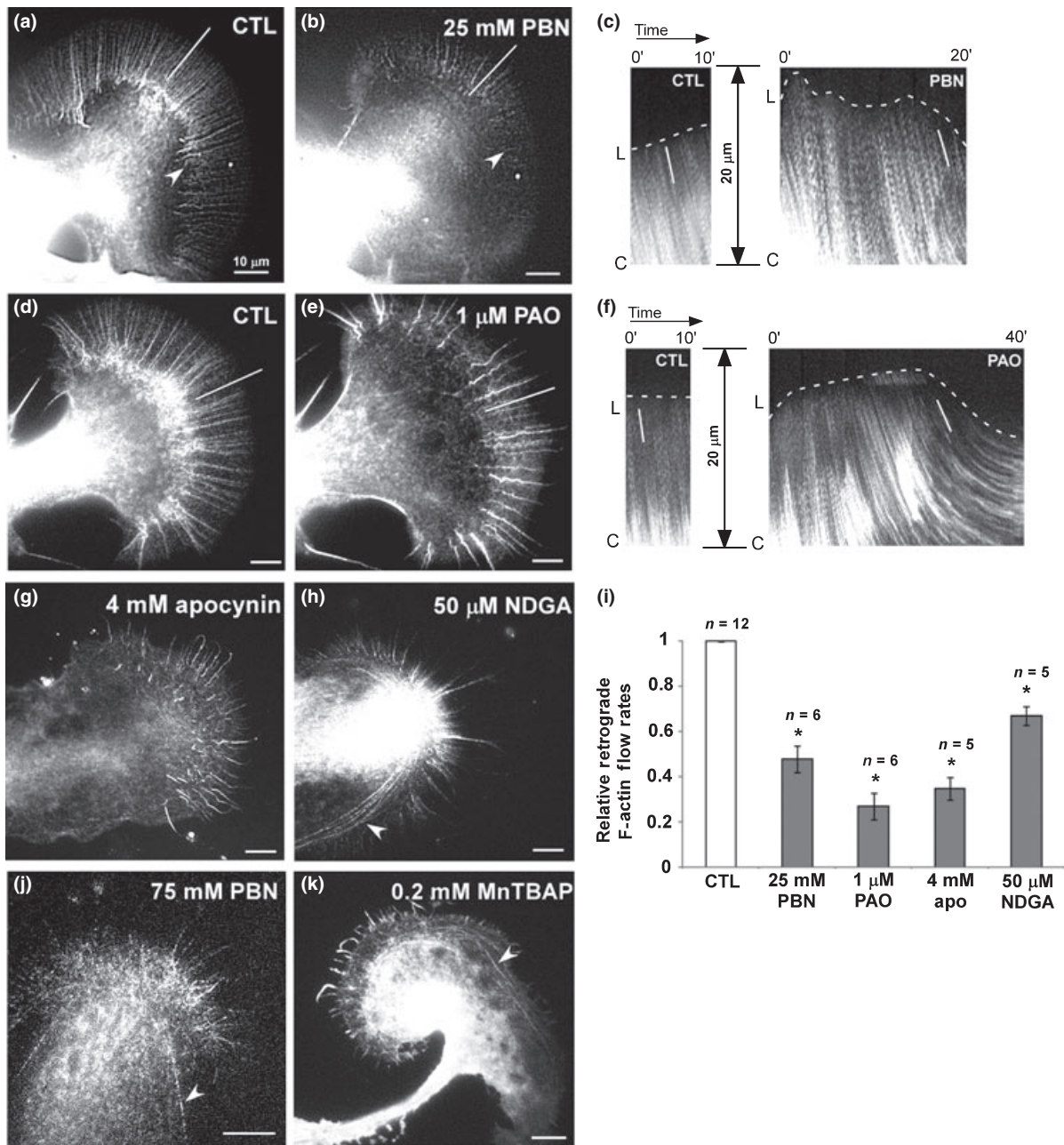


Fig. 4 ROS depletion affects F-actin dynamics. (a) F-actin dynamics of control growth cone. Neurons were injected with 20 μ M Alexa 568-phalloidin, and time lapse movies were acquired using FSM (Video S7). White line demarks lamellipodia region used for kymographs shown in (c). (b) Same growth cone after 20 min in 25 mM PBN. Note the progressive decrease in F-actin content in the P domain (Video S7). Arrowhead indicates forward movement of actin recycling zone. (c) Kymographs of actin speckles taken in the P domain as indicated with white lines in (a) and (b) reveal leading edge protrusion in control and progressive decrease in F-actin flow from initial control rate of 3.6 μ m/min to 2.1 μ m/min after PBN treatment (white lines in kymograph). (d) Actin FSM image of another control growth cone. (e) Same growth cone after treatment with 1 μ M PAO for 30 min, which causes disassembly of the actin cytoskeleton and forward shift of the

recycling zone (Video S8; image is shown after 25 min). A temporary lengthening of filopodial bundles occurred simultaneously with flow reduction. (f) Kymographs of actin speckles taken in P domain as indicated with white lines in (d) and (e) show a decrease in flow rates from 4.0 μ m/min in control to 1.5 μ m/min after PAO treatment. (g) 4 mM apocynin treatment caused a decrease in actin flow rates, filopodial lengthening and finally F-actin disassembly (Video S9). (h) 50 μ M NDGA resulted in an aggregation of actin arcs (arrowhead) (Video S10). (i) Quantification of actin retrograde flow rates. *T*-test: **p* < 0.005; *n* = number of growth cones. (j) 75 mM PBN resulted in an aggregation of actin arcs and contractile effects, similar to NDGA treatment (arrowhead) (Video S11). (k) Treatment with 0.2 mM MnTBAP resulted in temporary filopodia lengthening, arc aggregation (arrowhead) and overall network disassembly. Scale bars: 10 μ m.

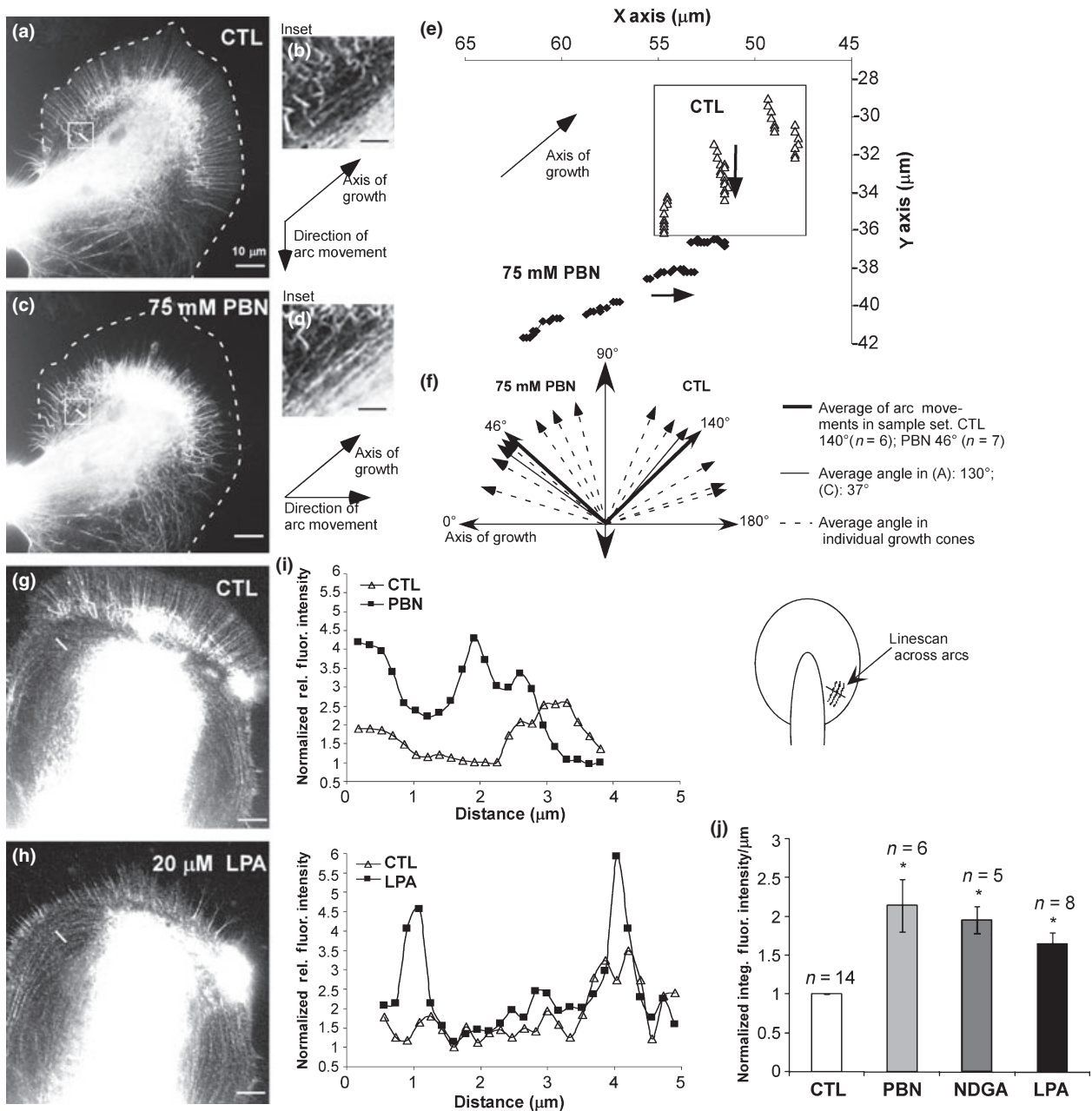


Fig. 5 ROS depletion affects actin arc movement and aggregation. (a) Actin FSM image of control growth cone. Filopodial actin bundles in P domain and actin arcs in T zone (marked with white box) undergo retrograde flow (Video S11). (b) Inset shows actin arcs marked in (a). In control conditions, arcs move retrogradely with respect to the axis of growth (Video S12). (c) The same growth cone treated for 3 min with 75 mM PBN (Video S11). We observed inhibition of F-actin assembly at the leading edge and retraction of the F-actin network towards the C domain. (d) Inset shows arc aggregation in 75 mM PBN. A brief tugging of actin arcs towards the axis of growth occurred before retraction of the F-actin network (Video S12). (e) Four speckles on actin arcs were tracked over 10 s intervals in control (open triangles) and 75 mM PBN (closed diamonds) conditions, respectively. (f) Angle plots of arc movements with respect to axis of growth from seven growth cones

(dashed arrows represent average angle per growth cone). Treatment with 75 mM PBN resulted in tugging of arcs towards the direction of growth at angles of less than 90°. Angles in control were always greater than 90°. Thin solid lines represent example shown in (a) and (c). (g) Actin FSM image of control growth cone. (h) 20 μM LPA treatment for 15 min resulted in increased arc aggregation. (i) Line scans across arcs marked by short white lines in (a), (c), (g), and (h) show arc aggregation by increased normalized relative fluorescence intensities after PBN and LPA treatment, respectively, relative to controls. (j) Integrated fluorescence intensities along the line scan per μm were normalized against control conditions. (*n* = number of growth cones). T-test: **p* < 0.01. Scale bars: 10 μm (in a, c, g, h); 5 μm (in b, d).

significant increases in F-actin signals when compared to the control condition before drug application. While LPA increased actin arc density by 65%, ROS depletion by PBN and NDGA raised actin arc signals by 115% and 96%, respectively (Fig. 5j). Thus, our results suggest that strong ROS depletion in growth cones results in increased actomyosin contractility similarly to LPA, presumably through Rho-activation.

ROS depletion increases Rho activity and decreases PY levels

Since ROS depletion had similar effects on F-actin dynamics in growth cones as Rho activation, we next tested whether ROS depletion increases Rho activity. Therefore, we performed a biochemical active Rho pull-down assay from *Aplysia* CNS tissue (Fig. 6). Total *Aplysia* CNS tissue was incubated in the presence or absence of 75 mM PBN, using 20 μ M LPA known to activate Rho as a positive control (Jalink *et al.* 1994). Both LPA and PBN increased Rho activity in CNS tissue when compared to untreated control tissue (Fig. 6a). Quantification of three independent experiments revealed that ROS depletion by PBN caused 1.7-fold increase in Rho activity compared to controls (*t*-test, $p = 0.07$; Fig. 6b), while LPA activated Rho by 2.7-fold ($p < 0.05$).

Since ROS are known to inhibit protein tyrosine phosphatases and activate protein tyrosine kinases (Meng *et al.* 2002; Chiarugi 2005), we tested whether the treatments with the ROS reagents affect the total PY levels in bag cell growth cones (Fig. 7). Under control conditions, PY immunolabeling was punctate in all growth cone regions with increased

signals in filopodia tips and along the leading edge (Fig. 7a), which is in agreement with our previous report (Suter and Forscher 2001). Treatment with 50 mM PBN, 1 μ M PAO, 4 mM apocynin, and 50 μ M NDGA abolished the PY enrichment at the leading edge and decreased total PY levels in the P domain by 52–62% when compared to controls, while rotenone treatment had no effect (Fig. 7b–g). Although NDGA treatment abolished the PY enrichment at the leading edge, it did not affect the PY signals at filopodial tips. Thus, we observed a direct correlation between ROS and global PY levels in *Aplysia* growth cones, suggesting a potential involvement of protein tyrosine phosphatases and/or kinases in the ROS-controlled cytoskeletal dynamics.

ROS depletion reduces growth cone formation and neurite outgrowth

In order to assess whether the changes in actin structure and dynamics induced by ROS depletion play a physiological role in growth cone formation and neurite outgrowth, we cultured bag cell neurons overnight in the presence and absence of various ROS reagents (Fig. 8). While $78 \pm 6\%$ of the control neurons displayed healthy growth cones after one day in culture (Fig. 8a-i and c), only $20 \pm 5\%$ of the cells cultured in 20 mM PBN had growth cones, which were smaller and flatter than in controls (Fig. 8b-i and c). After two days in culture, control neurons had more and longer neurites than on day one, and the percentage of growth cone-bearing cells increased to $91 \pm 3\%$ (Fig. 8a-ii and c). To assess whether growth inhibition by ROS depletion is reversible, we washed neurons grown in 20 mM PBN after one day with control medium. After PBN washout, $66 \pm 8\%$ of all cells exhibited growth cones on day two, which is not significantly different from control cells after one day in culture (Fig. 8b-ii and c; *t*-test: $p > 0.05$). Similarly, ROS depletion by overnight treatment of bag cell neurons with 500 nM PAO, 2 mM apocynin and 25 μ M NDGA reduced the percentage of neurons elaborating growth cones on day 1 after cell plating (Fig. 8c). While washout of apocynin resulted in a similar recovery as PBN washout ($69 \pm 11\%$), growth inhibition by overnight treatment with PAO and NDGA was not reversible.

We then assessed total neurite outgrowth under the same conditions (Fig. 8d and e). Only 30% of cells cultured overnight in 20 mM PBN had neurites of at least 50 μ m in total length, in contrast to 61% of control neurons. PBN washout after one day resulted in 77% of all cells bearing neurites on day 2, while 90% of control neurons have neurites on day 2 (Fig. 8d). As with growth cone formation, apocynin treatment reduced neurite outgrowth in a reversible manner, while neurite outgrowth inhibition by PAO and NDGA was irreversible (Fig. 8e). In summary, these findings suggest that ROS have an important physiological role in neurite outgrowth and regeneration and that NADPH oxidases and lipoxygenases are two important sources for ROS mediating these functions.

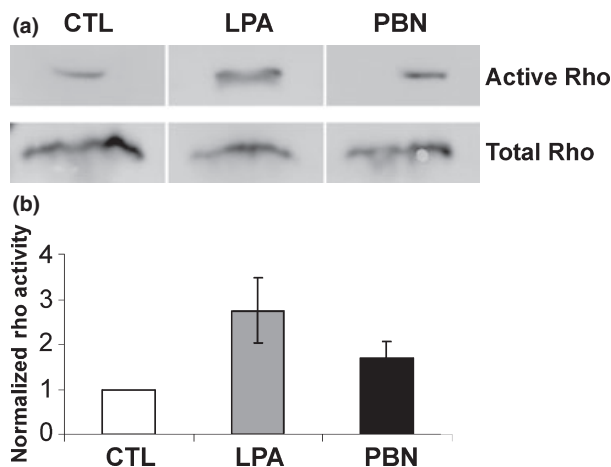


Fig. 6 PBN treatment increases Rho activity in *Aplysia* CNS tissue. (a) Western blot analysis of total and active Rho, as assessed by rhotekin-pull down assay. Total *Aplysia* CNS tissue was incubated in LIS-ASW only, with 20 μ M LPA or 75 mM PBN for 1 h. (b) Densitometric quantification of Rho activity (active/total Rho) in three independent experiments. Both LPA treatment and PBN increased Rho activity relative to control.

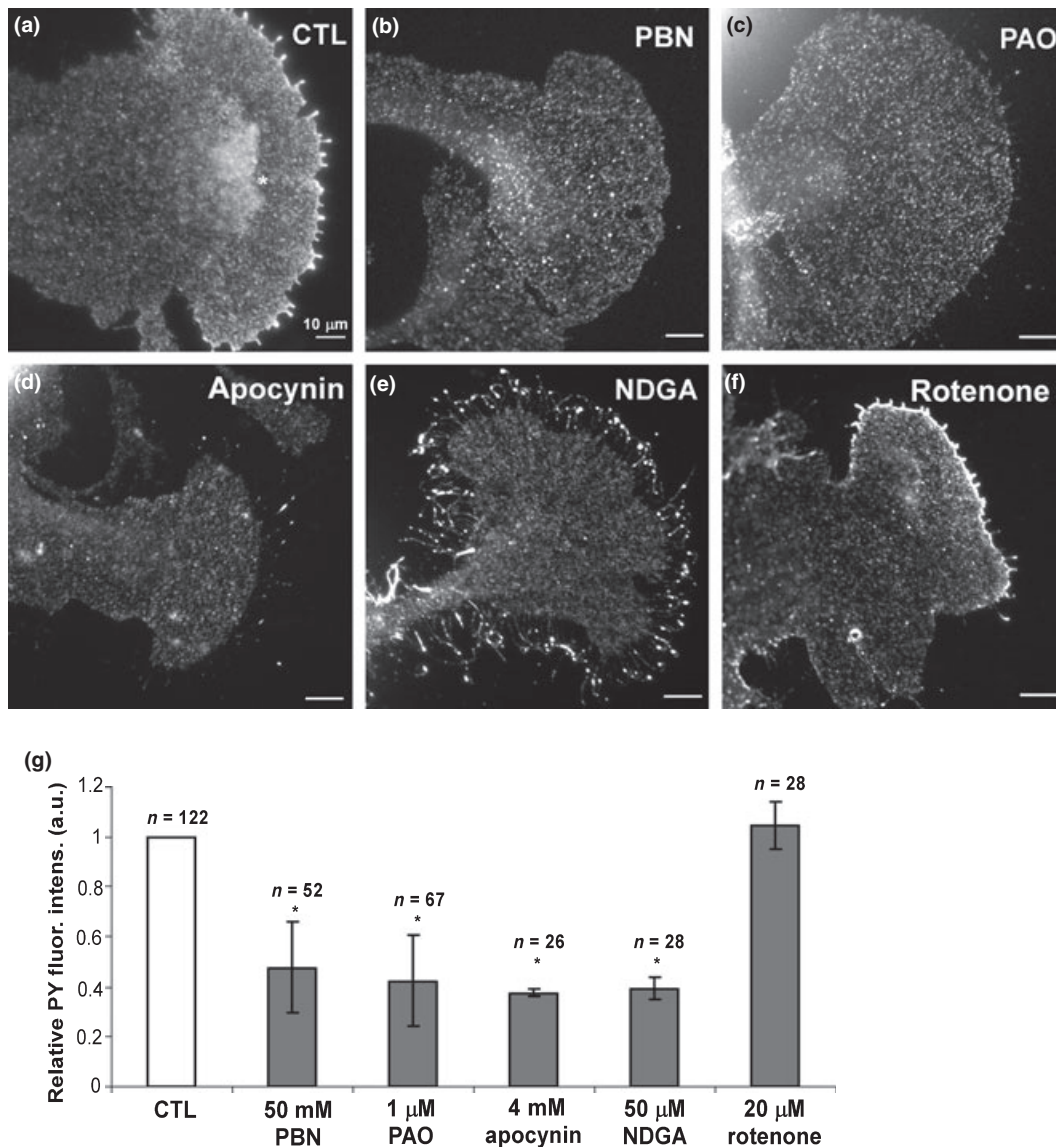


Fig. 7 Phosphotyrosine levels are decreased after ROS depletion. (a) Control growth cone labeled for total phosphotyrosine (PY) with monoclonal antibody 4G10. PY signals are increased at filopodia tips, leading edge and T zone ruffles (asterisk). 50 mM PBN (b), 1 μM PAO (c), 4 mM apocynin (d), and 50 μM NDGA (e) decreased PY signals in general and particularly along the leading edge. Note: NDGA treatment did not decrease PY levels in filopodia tips. (f) 20 μM rotenone

did not affect PY signals in P domain, leading edge or filopodia tips. (g) Quantification of PY levels in the P domain of growth cones reveals that 50 mM PBN, 1 μM PAO, 4 mM apocynin, and 50 μM NDGA decreased ROS levels by 52%, 58%, 62%, and 60%, respectively. Data are from three independent experiments. *T*-test: * $p < 0.05$ (n = number of growth cones). Scale bars: 10 μm.

Discussion

Besides the well-known damaging effects of ROS, specific signaling functions have been attributed to ROS in the nervous system, including regulation of programmed cell death (Maher and Schubert 2000) and long-term potentiation (Knapp and Klann 2002). Here, we provide the first evidence that a balance of physiological ROS levels is critical for maintaining a highly organized and dynamic F-actin cytoskeleton necessary for growth cone motility and neurite

outgrowth. Thus, similarly to non-neuronal cells, neurons have evolved to use ROS as second messengers for development and normal physiology.

ROS levels control F-actin structure and dynamics in growth cones

In the present study, we provide evidence that physiological ROS levels are critical for regulating F-actin dynamics in the growth cone. Lowering ROS levels with either a general scavenger or by inhibiting NADPH oxidases and lipoxygen-

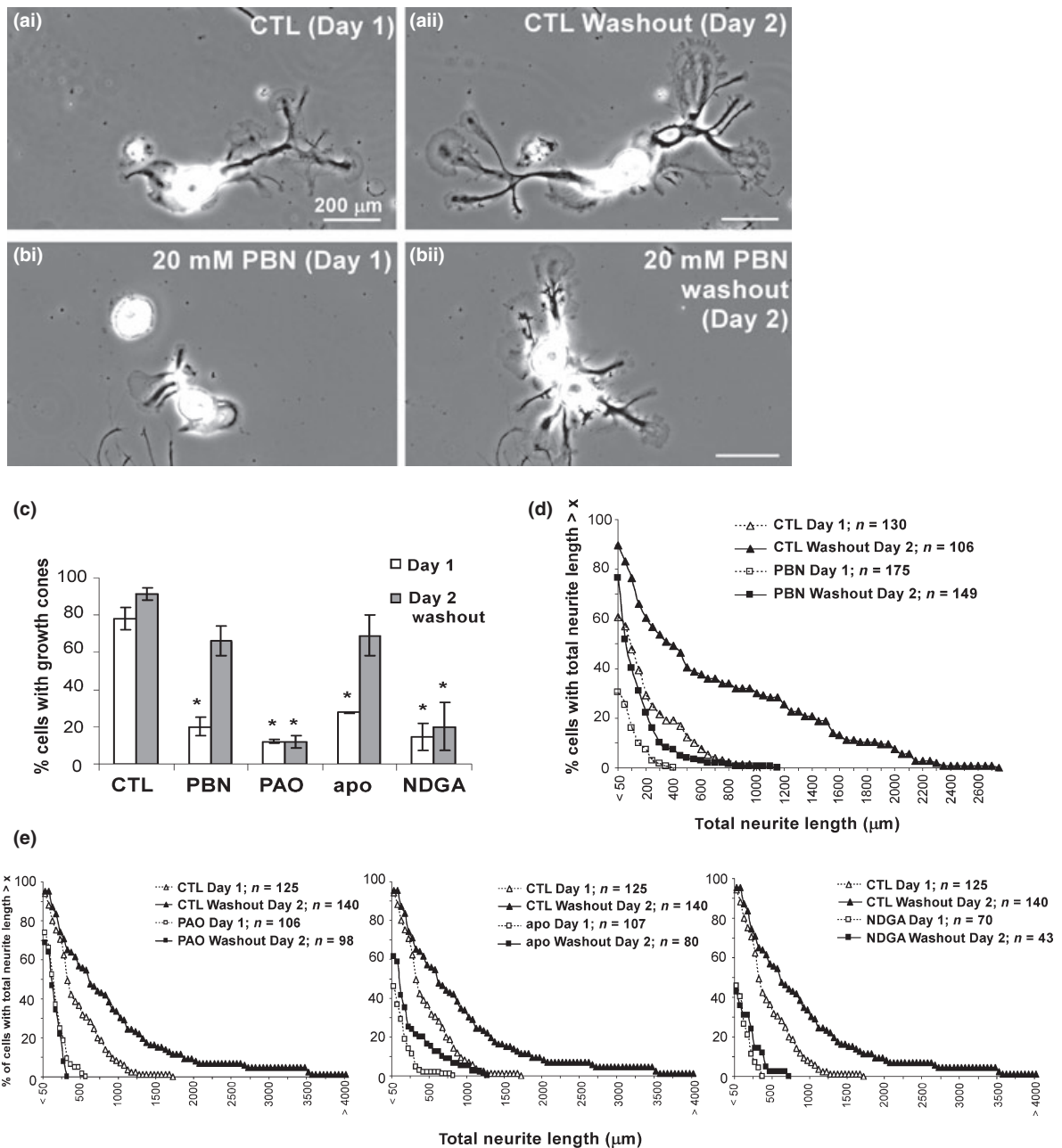


Fig. 8 ROS depletion reduces growth cone formation and neurite outgrowth. (a-i) Low magnification phase contrast image of a bag cell neuron with growth cones after one day in L15-ASW control condition. (a-ii) The same neuron imaged two days after plating had more, larger growth cones and longer neurites. (b-i) Neurons cultured for one day in 20 mM PBN had fewer, smaller and flatter growth cones at the ends of shorter neurites compared to controls. (b-ii) One day after PBN washout, the same cells have more, robust growth cones and longer neurites. The two cell bodies shown in (b-i) moved together between day one and two. (c) Quantification of percentage of cells that develop growth cones after one day in control medium, 20 mM PBN, 500 nM PAO, 2 mM apocynin and 25 μM NDGA (white bars) and on day 2 after washout of drugs between day 1 and 2 (gray bars). Between 43 and 255 cells were analyzed per condition in four independent

experiments. *T*-test: * $p < 0.05$. (d and e) Lowering ROS levels decreases neurite outgrowth. Population distribution of total neurite length per cell in control, 20 mM PBN (d), 500 nM PAO (e), 2 mM apocynin (e) and 25 μM NDGA (e) conditions on day one and on day 2 after washout. There was a significant decrease in total neurite length in neurons cultured in the presence of ROS drugs (open squares) when compared to L15-ASW control (open triangles) on day 1. PBN and apocynin effects were partially reversible, while PAO and NDGA effects were not. Quantifications in (c), (d) and (e) were carried out with the same cells (n = number of cells). Most neurons have pre-existing processes at the time of plating, explaining the differences in percentages of cells with growth cones and short neurites in some of the drug conditions. Scale bars: 200 μm.

ases, affected actin structure and dynamics similarly, although some slight differences were observed. The major effects were: (i) Reduced ruffling activity in the T zone; (ii) Inhibition of actin assembly at the leading edge; (iii) Attenuation of retrograde actin flow; (iv) Increase in Rho-dependent arc contractility; (v) Disassembly of actin filaments. Thus, ROS depletion generally reduces the protrusive while increasing the contractile activity of the growth cone. Accordingly, we would expect that physiological ROS levels promote actin assembly and leading edge protrusion. The slightly distinct actin effects induced by the various ROS reagents are likely because of the different ROS sensitivity of specific actin processes as well as because of the localization of different ROS sources in the growth cone. For example, increase in arc contractility and inhibition of actin assembly could be observed only upon fast and strong reduction of ROS levels with 75 mM PBN and 0.2 mM MnTBAP (Fig. 4j and k). In 25 mM PBN, however, the actin cytoskeleton gradually disassembles before significant increases in arc contractility and assembly inhibition occur. This could also explain the C domain extension observed in 25 mM PBN but not in 75 mM PBN.

We also observed different effects on actin dynamics when inhibiting specific ROS sources. NADPH oxidase inhibition resulted in reduced actin flow, inhibition of actin assembly at the leading edge and ultimately disassembly of both actin networks and bundles (Fig. 4; Videos S8 and S9). Prolonged treatment with NADPH oxidase inhibitors reduced actin assembly in filopodial tips. NADPH oxidases are expressed in both central and peripheral neurons (Hilburger *et al.* 2005; Tejada-Simon *et al.* 2005); however, growth cone localization has not been demonstrated so far. Based on our results, we speculate that NADPH oxidases are localized to the plasma membrane of the lamellipodia and potentially enriched along the leading edge of growth cones where they control assembly of actin networks and bundles. Such findings would be consistent with the localization of NADPH oxidases in focal complexes of lamellipodia, in membrane ruffles and at the leading edge of migrating endothelial cells (Ushio-Fukai 2006).

Lipoxygenase inhibition did not inhibit actin assembly in filopodial tips and rather promoted filopodial lengthening (Figs 3c and 4h). Furthermore, NDGA treatment caused actin arc accumulation similar to 75 mM PBN (Fig. 5), suggesting a role of lipoxygenase-derived ROS in the regulation of actomyosin-contraction in the T zone. Although lipoxygenases have not been localized to growth cones so far, there is experimental evidence that they are involved in semaphorin 3A-induced growth cone collapse of rat dorsal root ganglion neurons (Mikule *et al.* 2002) and netrin-1-mediated repulsive growth cone turning of *Xenopus* spinal cord neurons (Nishiyama *et al.* 2003). Thus, NADPH oxidases and lipoxygenases appear to have overlapping and distinct functions with respect to regulation of actin dynam-

ics. Since ROS are short-lived and diffusible, the detailed localization of NADPH oxidases and lipoxygenases in growth cones appears to be critical and will be an interesting avenue for future investigations. Finally, our results demonstrate that mitochondria-derived ROS do not appear to play a role in the regulation of actin structure and dynamics in growth cones. While in previous studies rotenone treatment resulted in both increased (Barrientos and Moraes 1999) and decreased cellular ROS levels (Thompson *et al.* 2007), cytoplasmic levels in the P domain of rotenone-treated *Aplysia* growth cones were not significantly different from controls.

In summary, we found that reduced ROS levels cause decreased actin assembly, retrograde flow and increased arc contractility in neuronal growth cones. These findings are in agreement with results from fibroblasts, endothelial cells and macrophages, although previous studies did not visualize actin dynamics (Moldovan *et al.* 2006; Chiarugi and Fiaschi 2007). In these non-neuronal cells, experimental elevation of total ROS increased F-actin content, while reducing ROS levels by inhibition of NADPH oxidases and lipoxygenases decreased actin assembly, cell motility and spreading but increased stress fiber formation (Crawford *et al.* 1996; Zhao and Davis 1998; Moldovan *et al.* 2000; Miller *et al.* 2001; Chiarugi *et al.* 2003; Nimnual *et al.* 2003; Wojciak-Stothard *et al.* 2005; Alexandrova *et al.* 2006; Fiaschi *et al.* 2006). Thus, ROS regulate actin dynamics in different cell types.

Potential targets of ROS in the growth cone cytoskeleton

A number of proteins are regulated by reversible oxidation through ROS, including protein tyrosine phosphatases, both receptor and non-receptor tyrosine kinases (e.g., epidermal growth factor receptor and Src), as well as actin itself (Meng *et al.* 2002; Chiarugi 2005; Moldovan *et al.* 2006; Chiarugi and Fiaschi 2007). We will discuss potential target proteins that regulate various aspects of actin dynamics in *Aplysia* growth cones in light of previous findings on ROS-mediated actin reorganization in fibroblasts and endothelial cells. Which proteins involved in actin assembly could be targeted by ROS? Rac1 is a key regulator of actin assembly processes (Etienne-Manneville and Hall 2002), thus a likely candidate. Indeed Rac1 activity is decreased in endothelial cells during hypoxia, while increased during reoxygenation (Wojciak-Stothard *et al.* 2005). Furthermore, antioxidants reduced Rac1 activity in fibroblasts (Alexandrova *et al.* 2006). There are a number of additional potential ROS target proteins involved in regulating actin assembly including Src tyrosine kinase and cofilin (Alexandrova *et al.* 2006; Moldovan *et al.* 2006; Chiarugi and Fiaschi 2007).

All experimental treatments that reduced cytoplasmic ROS levels in the growth cone also reduced PY levels in the P domain and along the leading edge (Figs 1 and 7). Since ROS inhibit protein tyrosine phosphatases and activate protein tyrosine kinases (Meng *et al.* 2002; Chiarugi 2005),

tyrosine phosphorylation is likely involved in ROS-mediated regulation of actin assembly. Although PAO can also inhibit tyrosine phosphatases at concentrations of 10 μM and higher (Le Cabec and Maridonneau-Parini 1995), we believe that the effects observed at concentrations of 1 μM and lower are largely through inhibition of NADPH oxidases and not tyrosine phosphatases. Evidence for this is given by the decreased PY levels after treatment with 1 μM PAO, which could be because of reduced ROS-mediated phosphatase inhibition. Furthermore, our PAO data are consistent with results obtained with an alternative NADPH oxidase inhibitor, apocynin.

When growth cones were treated with NDGA, we observed initial filopodia lengthening similarly to other treatments that reduce ROS levels. However, in contrast to NADPH oxidase inhibition and PBN treatment, NDGA-treated filopodia maintained their length, contained F-actin and PY proteins at the tips (Figs 3c-iii and 7e). These findings suggest that lipoxygenase-derived ROS may not control actin assembly at filopodia tips, but along the leading edge of lamellipodia. Since activated Src is also concentrated at filopodia tips (Suter *et al.* 2004; Robles *et al.* 2005), we hypothesize that ROS-mediated Src activation could be a major signaling pathway leading to actin assembly at the filopodia tips and leading edge. Finally, redox regulation of actin itself has been proposed as a potential mechanism for dynamic actin reorganization during integrin-mediated cell adhesion (Fiaschi *et al.* 2006). However, more work is needed to dissect the molecular details of actin assembly regulation by ROS.

Retrograde actin flow rates were decreased upon ROS depletion. Since myosin II motor activity largely drives actin flow in growth cones (Medeiros *et al.* 2006), we believe that reduced ROS levels may result in actomyosin interactions that are too tight and do not allow effective force production, since integrin-induced ROS cause actin oxidation and actomyosin disassembly in fibroblasts (Fiaschi *et al.* 2006). Furthermore, strong reduction of ROS levels with 75 mM PBN increased contractility of T zone arcs as evidenced by forward tugging of arcs, increased arc density, ripping apart of actomyosin networks and collapse of peripheral actin into the C domain. Since arc contractility is regulated by Rho GTPase (Zhang *et al.* 2003), we speculated that lowering ROS levels could increase Rho activity. Indeed Rho activity was increased in total CNS lysates after PBN treatment. How could ROS levels control Rho activity? A potential pathway from Rac1-mediated superoxide production to down-regulation of Rho activity has been reported for integrin-mediated spreading of HeLa cells (Nimnual *et al.* 2003). It involves ROS-mediated inhibition of low-molecular weight protein tyrosine phosphatase, which leads to phosphorylation and activation of p190 Rho GTPase activating protein, followed by reduced Rho activity. Similarly, reduced ROS levels resulted in Rho activation followed by actin stress fiber

formation, dispersion of adherens junctions and increased endothelial permeability in fibroblasts and endothelial cells (Wojciak-Stothard *et al.* 2005; Alexandrova *et al.* 2006). In summary, we speculate that physiological ROS levels are necessary to promote Rac1-dependent actin assembly leading to protrusion, while reducing Rho-dependent actomyosin contractility leading to growth cone retraction.

ROS in neurite outgrowth

Reduced ROS levels by overnight treatment with either PBN or NADPH oxidase or lipoxygenase inhibitors significantly inhibited growth cone formation and neurite outgrowth. Thus, physiological ROS levels appear to have a positive effect on neurite outgrowth of primary neurons in culture through regulation of the actin cytoskeleton. Our findings are consistent with previous studies demonstrating that ROS can act as a positive signal mediator in neuron-like cell lines; for example, in nerve growth factor-induced neurite outgrowth of PC-12 cells (Suzukawa *et al.* 2000).

In summary, similarly to several other physiological systems, ROS emerge as Janus-faced signaling molecules in the nervous system as well. While a large body of evidence revealed the damaging effects of ROS in disease states, including spinal cord injury and neurodegeneration, ROS also have 'positive' signaling functions in the nervous system, such as in synaptic function and plasticity, and neurite outgrowth. It will be of great interest to dissect which of the many axonal guidance receptors affect cytoskeletal dynamics via ROS signaling pathways.

Acknowledgements

The p1D9 anti-rho monoclonal antibody developed by Dr. Susan Parkhurst was obtained by the Developmental Studies Hybridoma Bank developed under the auspices of the NICHD and maintained by The University of Iowa, Department of Biological Sciences, Iowa City, IA 52242.

We thank Dr. Donald Ready as well members of the Suter lab for comments on the manuscript. We also thank Corinne Weisheit for assistance with MnTBAP experiments. This work was supported by grants from the NIH (R01 NS049233) and the Bindley Bioscience Center at Purdue University to D.M.S. V. M. was partially supported by fellowships through the PULSE and PUN Integrative Neuroscience graduate programs at Purdue University.

Supporting information

Additional Supporting Information may be found in the online version of this article:

Video S1. DIC time lapse movie of growth cone in control (CTL) condition for 3.3 min followed by treatment with 25 mM PBN for 20 min (Fig. 2b-i,ii). PBN treatment caused an initial burst of filopodial growth, flattening of the T zone, disappearance of actin bundles in the P domain and forward movement of the C domain boundary. Time compression: 100 \times . Scale bar: 10 μm .

Video S2. DIC time lapse movie of growth cone in control (CTL) condition for 3.3 min treated followed by treatment with 75 mM PBN for 5 min (Fig. 2c-i,ii). Besides flattening of the T zone and disappearance of actin bundles, the higher PBN dose also caused a slight retraction of the C domain boundary and reduced growth cone dynamics. Time compression: 100×. Scale bar: 10 μ m.

Video S3. DIC time lapse movie of growth cone in control (CTL) condition for 3.3 min followed by treatment with 1 μ M PAO for 10 min (Fig. 3a-i,ii). Besides flattening of the T zone and disappearance of actin bundles, PAO also caused a slight retraction of the C domain boundary. In addition, growth cone lamellipodia dynamics were reduced. Time compression: 100×. Scale bar: 10 μ m.

Video S4. DIC time lapse movie of growth cone in control (CTL) condition for 3.3 min followed by treatment with 4 mM apocynin for 10 min (Fig. 3b-i,ii). Apocynin caused flattening of the T zone, extension of the C domain and disappearance of actin bundles. Time compression: 100×. Scale bar: 10 μ m.

Video S5. DIC time lapse movie of growth cone in control (CTL) condition for 3.3 min followed by treatment with 50 μ M NDGA for 10 min (Fig. 3c-i,ii). NDGA caused flattening of the T zone, disappearance of actin bundles and filopodia lengthening. Time compression: 100×. Scale bar: 10 μ m.

Video S6. DIC time lapse movie of growth cone in control (CTL) condition for 3.3 min followed by treatment with 20 μ M Rotenone for 10 min (Fig. 3d-i,ii). Rotenone treatment did not result in major morphological changes besides a slight splaying of the C domain. Time compression: 100×. Scale bar: 10 μ m.

Video S7. F-actin dynamics time lapse movie of growth cone labeled with Alexa 568-phalloidin in control (CTL) condition for 3.3 min followed by treatment with 25 mM PBN for 20 min (Fig. 4a and b). PBN treatment caused initial leading edge and filopodial protrusion, slowing of F-actin flow, disassembly of F-actin structures and narrowing of the P domain. Time compression: 100×. Scale bar: 10 μ m.

Video S8. F-actin dynamics time lapse movie of growth cone labeled with Alexa 568-phalloidin in control (CTL) condition for 3.3 min followed by treatment with 1 μ M PAO for 30 min (Fig. 4d and e). PAO treatment resulted in slowing of actin flow, temporary lengthening of filopodia, forward movement of the recycling zone and ultimately disassembly of the actin cytoskeleton. Time compression: 100×. Scale bar: 10 μ m.

Video S9. F-actin dynamics time lapse movie of growth cone labeled with Alexa 568-phalloidin in control (CTL) condition for 3.3 min followed by treatment with 4 mM apocynin for 25 min (Fig. 4g). Apocynin treatment resulted in slowing of actin flow, temporary lengthening of filopodia, forward movement of the recycling zone and ultimately disassembly of the actin cytoskeleton. Time compression: 100×. Scale bar: 10 μ m.

Video S10. F-actin dynamics time lapse movie of growth cone labeled with Alexa 568-phalloidin in control (CTL) condition for 3.3 min followed by treatment with 50 μ M NDGA for 20 min (Fig. 4h). NDGA treatment resulted in reduced F-actin assembly, retraction of the actin network and contractile effects on F-actin arcs and networks in the T zone, similar to 75 mM PBN treatment. Time compression: 100×. Scale bar: 10 μ m.

Video S11. F-actin dynamics time lapse movie of growth cone labeled with Alexa 568-phalloidin in control (CTL) condition for 3.3 min followed by treatment with 75 mM PBN for 5 min (Fig. 5a

and c). PBN treatment resulted in inhibition of actin assembly, retraction of the actin network and contractile effects on actin arcs and networks in the T zone. Time compression: 100×. Scale bar: 10 μ m.

Video S12. F-actin dynamics time lapse movie of arc movements in the T zone (Fig. 5b and d) in control (CTL) conditions for 2 min and in 75 mM PBN for 2 min. In control conditions, arcs move retrogradely, while forward tugging and arc aggregation was observed in PBN. Time compression: 100×. Scale bar: 5 μ m.

Please note: Wiley-Blackwell are not responsible for the content or functionality of any supporting materials supplied by the authors. Any queries (other than missing material) should be directed to the corresponding author for the article.

References

- Abo A., Pick E., Hall A., Totty N., Teahan C. G. and Segal A. W. (1991) Activation of the NADPH oxidase involves the small GTP-binding protein p21rac1. *Nature* **353**, 668–670.
- Alexandrova A. Y., Kopnin P. B., Vasiliev J. M. and Kopnin B. P. (2006) ROS up-regulation mediates Ras-induced changes of cell morphology and motility. *Exp. Cell Res.* **312**, 2066–2073.
- Barrientos A. and Moraes C. T. (1999) Titrating the effects of mitochondrial complex I impairment in the cell physiology. *J. Biol. Chem.* **274**, 16188–16197.
- Bedard K. and Krause K. H. (2007) The NOX family of ROS-generating NADPH oxidases: physiology and pathophysiology. *Physiol. Rev.* **87**, 245–313.
- Chang S., Rathjen F. G. and Raper J. A. (1987) Extension of neurites on axons is impaired by antibodies against specific neural cell surface glycoproteins. *J. Cell Biol.* **104**, 355–362.
- Chiarugi P. (2005) PTPs versus PTKs: the redox side of the coin. *Free Radic. Res.* **39**, 353–364.
- Chiarugi P. and Fiaschi T. (2007) Redox signalling in anchorage-dependent cell growth. *Cell. Signal.* **19**, 672–682.
- Chiarugi P., Pani G., Giannoni E., Taddei L., Colavitti R., Raugei G., Symons M., Borrello S., Galeotti T. and Ramponi G. (2003) Reactive oxygen species as essential mediators of cell adhesion: the oxidative inhibition of a FAK tyrosine phosphatase is required for cell adhesion. *J. Cell Biol.* **161**, 933–944.
- Crawford L. E., Milliken E. E., Irani K., Zweier J. L., Becker L. C., Johnson T. M., Eissa N. T., Crystal R. G., Finkel T. and Goldschmidt-Clermont P. J. (1996) Superoxide-mediated actin response in post-hypoxic endothelial cells. *J. Biol. Chem.* **271**, 26863–26867.
- Cui Z. G., Kondo T. and Matsumoto H. (2006) Enhancement of apoptosis by nitric oxide released from alpha-phenyl-tert-butyl nitron under hyperthermic conditions. *J. Cell. Physiol.* **206**, 468–476.
- Duan Y., Gross R. A. and Sheu S. S. (2007) Ca²⁺-dependent generation of mitochondrial reactive oxygen species serves as a signal for poly(ADP-ribose) polymerase-1 activation during glutamate excitotoxicity. *J. Physiol.* **585**, 741–758.
- Etienne-Manneville S. and Hall A. (2002) Rho GTPases in cell biology. *Nature* **420**, 629–635.
- Fiaschi T., Cozzi G., Raugei G., Formigli L., Ramponi G. and Chiarugi P. (2006) Redox regulation of beta-actin during integrin-mediated cell adhesion. *J. Biol. Chem.* **281**, 22983–22991.
- Forscher P. and Smith S. J. (1988) Actions of cytochalasins on the organization of actin filaments and microtubules in a neuronal growth cone. *J. Cell Biol.* **107**, 1505–1516.
- Gallo G. (2006) RhoA-kinase coordinates F-actin organization and myosin II activity during semaphorin-3A-induced axon retraction. *J. Cell Sci.* **119**, 3413–3423.

- Gallo G. and Letourneau P. C. (2004) Regulation of growth cone actin filaments by guidance cues. *J. Neurobiol.* **58**, 92–102.
- Giniger E. (2002) How do Rho family GTPases direct axon growth and guidance? A proposal relating signaling pathways to growth cone mechanics. *Differentiation* **70**, 385–396.
- Grzywa E. L., Lee A. C., Lee G. U. and Suter D. M. (2006) High-resolution analysis of neuronal growth cone morphology by comparative atomic force and optical microscopy. *J. Neurobiol.* **66**, 1529–1543.
- Hilburger E. W., Conte E. J., McGee D. W. and Tammariello S. P. (2005) Localization of NADPH oxidase subunits in neonatal sympathetic neurons. *Neurosci. Lett.* **377**, 16–19.
- Jalink K., van Corven E. J., Hengeveld T., Morii N., Narumiya S. and Moolenaar W. H. (1994) Inhibition of lysophosphatidate- and thrombin-induced neurite retraction and neuronal cell rounding by ADP-ribosylation of the small GTP-binding protein Rho. *J. Cell Biol.* **126**, 801–810.
- Knapp L. T. and Klann E. (2002) Role of reactive oxygen species in hippocampal long-term potentiation: contributory or inhibitory? *J. Neurosci. Res.* **70**, 1–7.
- Kotake Y., Sang H., Miyajima T. and Wallis G. L. (1998) Inhibition of NF- κ B, iNOS mRNA, COX2 mRNA, and COX catalytic activity by phenyl-N-tert-butyl nitron (PBN). *Biochim. Biophys. Acta* **1448**, 77–84.
- Lambeth J. D. (2007) Nox enzymes, ROS, and chronic disease: an example of antagonistic pleiotropy. *Free Radic. Biol. Med.* **43**, 332–347.
- Le Cabec V. and Maridonneau-Parini I. (1995) Complete and reversible inhibition of NADPH oxidase in human neutrophils by phenylarsine oxide at a step distal to membrane translocation of the enzyme subunits. *J. Biol. Chem.* **270**, 2067–2073.
- Lee A. C., Decourt B. and Suter D. M. (2008) Neuronal cell cultures from Aplysia for high-resolution imaging of growth cones. *J. Vis. Experim.* **12**, doi: 10.3791/662.
- Lewis A. K. and Bridgman P. C. (1992) Nerve growth cone lamellipodia contain two populations of actin filaments that differ in organization and polarity. *J. Cell Biol.* **119**, 1219–1243.
- Luo J., Li N., Robinson J. P. and Shi R. (2002) The increase of reactive oxygen species and their inhibition in an isolated guinea pig spinal cord compression model. *Spinal Cord* **40**, 656–665.
- Maher P. and Schubert D. (2000) Signaling by reactive oxygen species in the nervous system. *Cell. Mol. Life Sci.* **57**, 1287–1305.
- Medeiros N. A., Burnette D. T. and Forscher P. (2006) Myosin II functions in actin-bundle turnover in neuronal growth cones. *Nat. Cell Biol.* **8**, 215–226.
- Meng T. C., Fukada T. and Tonks N. K. (2002) Reversible oxidation and inactivation of protein tyrosine phosphatases in vivo. *Mol. Cell* **9**, 387–399.
- Mikule K., Gatlin J. C., de la Houssaye B. A. and Pfenninger K. H. (2002) Growth cone collapse induced by semaphorin 3A requires 12/15-lipoxygenase. *J. Neurosci.* **22**, 4932–4941.
- Miller Y. I., Chang M. K., Funk C. D., Feramisco J. R. and Witztum J. L. (2001) 12/15-Lipoxygenase translocation enhances site-specific actin polymerization in macrophages phagocytosing apoptotic cells. *J. Biol. Chem.* **276**, 19431–19439.
- Moldovan L., Moldovan N. I., Sohn R. H., Parikh S. A. and Goldschmidt-Clermont P. J. (2000) Redox changes of cultured endothelial cells and actin dynamics. *Circ. Res.* **86**, 549–557.
- Moldovan L., Myhre K., Goldschmidt-Clermont P. J. and Satterwhite L. L. (2006) Reactive oxygen species in vascular endothelial cell motility. Roles of NAD(P)H oxidase and Rac1. *Cardiovasc. Res.* **71**, 236–246.
- Nimmual A. S., Taylor L. J. and Bar-Sagi D. (2003) Redox-dependent downregulation of Rho by Rac. *Nat. Cell Biol.* **5**, 236–241.
- Nishiyama M., Hoshino A., Tsai L., Henley J. R., Goshima Y., Tessier-Lavigne M., Poo M. M. and Hong K. (2003) Cyclic AMP/GMP-dependent modulation of Ca²⁺ channels sets the polarity of nerve growth-cone turning. *Nature* **423**, 990–995.
- Patel M. (1998) Inhibition of neuronal apoptosis by a metalloporphyrin superoxide dismutase mimic. *J. Neurochem.* **71**, 1068–1074.
- Reynolds I. J. and Hastings T. G. (1995) Glutamate induces the production of reactive oxygen species in cultured forebrain neurons following NMDA receptor activation. *J. Neurosci.* **15**, 3318–3327.
- Robles E., Woo S. and Gomez T. M. (2005) Src-dependent tyrosine phosphorylation at the tips of growth cone filopodia promotes extension. *J. Neurosci.* **25**, 7669–7681.
- Rochlin M. W., Dailey M. E. and Bridgman P. C. (1999) Polymerizing microtubules activate site-directed F-actin assembly in nerve growth cones. *Mol. Biol. Cell* **10**, 2309–2327.
- Salari H., Braquet P. and Borgeat P. (1984) Comparative effects of indomethacin, acetylenic acids, 15-HETE, nordihydroguaiaretic acid and BW755C on the metabolism of arachidonic acid in human leukocytes and platelets. *Prostaglandins Leukot. Med.* **13**, 53–60.
- Schaefer A. W., Kabir N. and Forscher P. (2002) Filopodia and actin arcs guide the assembly and transport of two populations of microtubules with unique dynamic parameters in neuronal growth cones. *J. Cell Biol.* **158**, 139–152.
- Stolk J., Hiltermann T. J., Dijkman J. H. and Verhoeven A. J. (1994) Characteristics of the inhibition of NADPH oxidase activation in neutrophils by apocynin, a methoxy-substituted catechol. *Am. J. Respir. Cell Mol. Biol.* **11**, 95–102.
- Sturgess N. C., Rustad A., Fonnum F. and Lock E. A. (2000) Neurotoxic effect of L-2-chloropropionic acid on primary cultures of rat cerebellar granule cells. *Arch. Toxicol.* **74**, 153–160.
- Suter D. M. and Forscher P. (2001) Transmission of growth cone traction force through apCAM-cytoskeletal linkages is regulated by Src family tyrosine kinase activity. *J. Cell Biol.* **155**, 427–438.
- Suter D. M., Errante L. D., Belotserkovsky V. and Forscher P. (1998) The Ig superfamily cell adhesion molecule, apCAM, mediates growth cone steering by substrate-cytoskeletal coupling. *J. Cell Biol.* **141**, 227–240.
- Suter D. M., Schaefer A. W. and Forscher P. (2004) Microtubule dynamics are necessary for SRC family kinase-dependent growth cone steering. *Curr. Biol.* **14**, 1194–1199.
- Suzukawa K., Miura K., Mitsushita J., Resau J., Hirose K., Crystal R. and Kamata T. (2000) Nerve growth factor-induced neuronal differentiation requires generation of Rac1-regulated reactive oxygen species. *J. Biol. Chem.* **275**, 13175–13178.
- Tabner B. J., Turnbull S., El-Agnaf O. and Allsop D. (2001) Production of reactive oxygen species from aggregating proteins implicated in Alzheimer's disease, Parkinson's disease and other neurodegenerative diseases. *Curr. Top. Med. Chem.* **1**, 507–517.
- Tejada-Simon M. V., Serrano F., Villasana L. E., Kanterewicz B. I., Wu G. Y., Quinn M. T. and Klann E. (2005) Synaptic localization of a functional NADPH oxidase in the mouse hippocampus. *Mol. Cell. Neurosci.* **29**, 97–106.
- Thannickal V. J. and Fanburg B. L. (2000) Reactive oxygen species in cell signaling. *Am. J. Physiol. Lung Cell Mol. Physiol.* **279**, L1005–L1028.
- Thomas C. E., Ohlweiler D. F., Taylor V. L. and Schmidt C. J. (1997) Radical trapping and inhibition of iron-dependent CNS damage by cyclic nitron spin traps. *J. Neurochem.* **68**, 1173–1182.
- Thompson R. J., Buttigieg J., Zhang M. and Nurse C. A. (2007) A rotenone-sensitive site and H₂O₂ are key components of hypoxia-sensing in neonatal rat adrenomedullary chromaffin cells. *Neuroscience* **145**, 130–141.
- Ushio-Fukai M. (2006) Localizing NADPH oxidase-derived ROS. *Sci. STKE* **349**, re8.

- Waterman-Storer C. M., Desai A., Bulinski J. C. and Salmon E. D. (1998) Fluorescent speckle microscopy, a method to visualize the dynamics of protein assemblies in living cells. *Curr. Biol.* **8**, 1227–1230.
- Wojciak-Stothard B., Tsang L. Y. and Haworth S. G. (2005) Rac and Rho play opposing roles in the regulation of hypoxia/reoxygenation-induced permeability changes in pulmonary artery endothelial cells. *Am. J. Physiol. Lung Cell Mol. Physiol.* **288**, L749–L760.
- Woo C. H., Eom Y. W., Yoo M. H., You H. J., Han H. J., Song W. K., Yoo Y. J., Chun J. S. and Kim J. H. (2000) Tumor necrosis factor- α generates reactive oxygen species via a cytosolic phospholipase A2-linked cascade. *J. Biol. Chem.* **275**, 32357–32362.
- Xu W., Chi L., Xu R., Ke Y., Luo C., Cai J., Qiu M., Gozal D. and Liu R. (2005) Increased production of reactive oxygen species contributes to motor neuron death in a compression mouse model of spinal cord injury. *Spinal Cord* **43**, 204–213.
- Zhang X. F., Schaefer A. W., Burnette D. T., Schoonderwoert V. T. and Forscher P. (2003) Rho-dependent contractile responses in the neuronal growth cone are independent of classical peripheral retrograde actin flow. *Neuron* **40**, 931–944.
- Zhao Y. and Davis H. W. (1998) Hydrogen peroxide-induced cytoskeletal rearrangement in cultured pulmonary endothelial cells. *J. Cell. Physiol.* **174**, 370–379.
- Zini I., Tomasi A., Grimaldi R., Vannini V. and Agnati L. F. (1992) Detection of free radicals during brain ischemia and reperfusion by spin trapping and microdialysis. *Neurosci. Lett.* **138**, 279–282.